Applied Catalysis B: Environmental 123–124 (2012) 414–423

Contents lists available at SciVerse ScienceDirect

Applied Catalysis B: Environmental

journal homepage: www.elsevier.com/locate/apcatb

Concurrent photoelectrochemical reduction of CO_2 and oxidation of methyl orange using nitrogen-doped TiO_2

Yen-Ping Peng[a], Yun-Ta Yeh[a], S. Ismat Shah[b,c], C.P. Huang[a,*]

[a] Department of Civil and Environmental Engineering, University of Delaware, Newark, DE, 19716, USA
[b] Department of Material Science Engineering, University of Delaware, Newark, DE, 19716, USA
[c] Department of Physics and Astronomy, University of Delaware, Newark, DE, 19716, USA

ARTICLE INFO

Article history:
Received 19 January 2012
Received in revised form 6 April 2012
Accepted 23 April 2012
Available online 28 April 2012

Keywords:
Photoelectrochemical
CO_2 reduction
Nitrogen-doped TiO_2
Kinetics

ABSTRACT

This study employed a novel material, nitrogen-doped TiO_2 thin film (NTTF), as a photoanode for the concurrent photoeletrochemical (PEC) reduction of CO_2 and oxidation of methyl Orange (MO). Under illumination, the onset potential of the total current was approximately 1.5 V (vs. SCE) and the maximum total current was around 0.65 mA at 2 V (vs. SCE). The photocurrent can be effectively driven to the counter electrode at this positive potential, which will decrease the recombination of photo-generated holes and electrons, leading to more electrons available for CO_2 reduction in the cathodic chamber and more holes for the oxidation of hazardous chemicals in the anodic chamber simultaneously. Formic acid, formaldehyde, methanol and methane were detected as the CO_2 reduction products at a Cu electrode in the $KHCO_3$ electrolyte. The first-order kinetic model was successfully applied to simulate the NTTF PEC reduction of CO_2. The reaction rate constant were 6.68×10^{-7}, 2.18×10^{-4}, 8.62×10^{-4} and 2.27×10^{-4} s^{-1}, for the formation of formic acid, formaldehyde, methanol, and methane, respectively. The maximum Faradaic efficiency was 5.01, 1.04, 5.41 and 7.83% for the generation of formic acid, formaldehyde, methanol, and methane, individually. In addition, the effect of initial CO_2 concentration on CO_2 reduction was also conducted in the presence of methanol (0, 20 and 40%). Results showed that methanol-containing electrolyte enhanced CO_2 solubility thereby suppressing hydrogen generation and favoring CO_2 reduction. Finally, the degradation of methyl orange was compared using PEC, photocatalytic (PC), electrochemical (EC) and direct photolysis (P) processes. The PEC process was able to achieve a 10-log versus less than 1-log of methyl orange degradation by all other methods studied within 60 min under otherwise similar conditions of pH, temperature, intensity and wavelength of light source. Results clearly demonstrated the potential of a sustainable technology for the concurrent reduction of CO_2 and oxidation of hazardous chemicals by the PEC process using solar energy.

1. Introduction

It has been suggested that carbon dioxide (CO_2) is one of the primary greenhouse gases responsible for current global warming. Recently, there are attempts to utilize CO_2 as natural resource, that is, as a feedstock rather than a waste product that requires costly disposal [1,2]. Chemical reduction of carbon dioxide is thermodynamically feasible in the presence of strong reducing agents such as metallic elements (Ti, Fe) and borohydride (BH_4^-)[3]. However, the process requires electron-donating chemicals. Therefore, to minimize or avoid use of chemicals, processes such as electrochemical [4–10], photocatalytic [11–17] and photoelectrochemical [18–22] have gained attention. Electrochemical CO_2 reduction is achievable using low-hydrogen-overpotential working electrode at which surface carbon dioxide can be reduced to formic acid, formaldehyde, methanol, and methane. Nevertheless, electrochemical reduction is not energy free; it still requires electricity. Photocatalytic reduction using photocatalysts such as TiO_2 can be promising alternative to electrochemical reduction of carbon dioxide. While photocatalytic conversion of carbon dioxide to methane and other energy-rich compounds is possible, the photocatalytic efficiency was generally low at less than 10%. This is because holes that are being generated at the same time as electrons can oxidize the reaction products or intermediates back to the parent compound, i.e., carbon dioxide in addition to rapid recombination with electrons. This has prompted several studies to use hole scavengers such as 2-propanol, methanol and ethanol to increase the yield [23]. However, the use of organic hole scavengers is counterproductive. This has prompted researchers to study photoelectrochemical process using visible light sensitivity materials to convert carbon dioxide to energy-rich organic compounds. The first use of photocatalyst as photocathode to photoelectrochemically reduce CO_2 can be dated back over 30 years ago [21]. Inoue et al. [18] examined the

* Corresponding author. Tel.: +1 302 831 8428; fax: +1 302 831 3640.
E-mail address: huang@udel.edu (C.P. Huang).

0926-3373/$ – see front matter © 2012 Elsevier B.V. All rights reserved.
http://dx.doi.org/10.1016/j.apcatb.2012.04.037

photoelectrocatalytic reduction of CO_2 in aqueous suspensions of TiO_2, ZnO, CdS, GaP, SiC and WO_3 powders. Furthermore, various p-type semiconductors including p-InP, p-GaP, p-GaAs, p-SiC and p-CdTe were investigated for CO_2 reduction [22,24–28]. These novel materials can utilize solar energy, a renewable and green energy, to generate electrons in sufficient quantity for CO_2 reduction. Among these materials, TiO_2 has been the most studied due to its attractive photocatalytic activity, chemical stability, nontoxicity, and low cost. However, TiO_2 having a high band gap between 3.2 and 3.4 eV is sensitive to UV light, which composes less than 5% of the solar spectrum. Herein, this study was to apply a nitrogen-doped TiO_2 thin film, prepared by pulsed laser deposition (PLD) method, as the photoanode in the PEC system [29,30]. The NTTF has a band gap of 2.0 eV and can be excited by the visible light. To the best of our knowledge, there is no reported use of N-doped TiO_2 thin film as photoanode for photoelectrochemical CO_2 reduction.

Many studies have reported photoelectrochemical CO_2 reduction using various photocatalysts, but only a few have dealt with the CO_2 reduction kinetics. Lo et al. [13] and Tan et al. [14] used Langmuir–Hinshelwood model to describe the kinetics of the formation of CO_2 reduction products. Koci et al. [31] subsequently modified the Langmuir–Hinshelwood model and predicted successfully the CO_2 reduction products in liquid and gas phases. Dey [30] reviewed chemical reduction of CO_2 using TiO_2 photocatalysts and reported that two reaction pathways all led to the formation of CH_4, viz. $CO_2 \rightarrow HCOOH \rightarrow HCHO \rightarrow CH_3OH \rightarrow CH_4$ and $CO_2 \rightarrow CO \rightarrow C \rightarrow CH_2 \rightarrow CH_4$. The former mechanism was based on the results obtained in condensed media, whereas the latter was based on the findings in photocatalytic reduction of CO_2 at high pressure using TiO_2 in suspension. The objective of the present study was to understand the mechanistic aspects of the photoelectrochemical CO_2 reduction processes by establishing the kinetic equations for the formation of pertinent CO_2 reduction products, namely, HCOOH, HCOH, CH_3OH and CH_4, for the first time using N-doped TiO_2 in thin film.

2. Experimental

2.1. Materials

Deionized water was prepared in the laboratory using a water-purification system (Mega-Pure System, model MP-290). Potassium bicarbonate, formaldehyde (purity >97%), methanol, acetonitrile (HPLC grade), sodium hydroxide, sulfuric acid were purchased from Fisher Scientific, USA. Sodium chloride (purity >99%), formic acid (purity >99%), and phosphoric acid (purity >85%) were purchased from ACROS, USA. 2,4-Dinitrophenylhydrazine (DNPH), and methyl orange (purity >85%) was purchased from Sigma–Aldrich, USA. A copper wire 1 mm in diameter from Fisher Scientific, USA, was curled to a coil of 0.9 cm in diameter and 35 cm (11 in.) in length and used as cathode. The light source was a 100-W Xe lamp with an average incident light intensity of 3.12 mW cm^{-2} measured by a high sensitivity thermal sensors (model 3A-P-SH-V1, OPHIR, USA).

2.2. Reduction of carbon dioxide and oxidation of methyl orange

Fig. 1 shows the schematic diagram of the photoelectrochemical (PEC) system. All PEC experiments were carried out in three-electrode mode at room temperature. A saturated calomel electrode (SCE) was selected as the reference electrode. A nitrogen-doped TiO_2 thin film (NTTF) was used as the working electrode (6.25 cm^2). Detailed procedures on the preparation and characterization of NTTF will be reported elsewhere [32]. Briefly, a pure TiO_2 target prepared from P25 Degussa particles

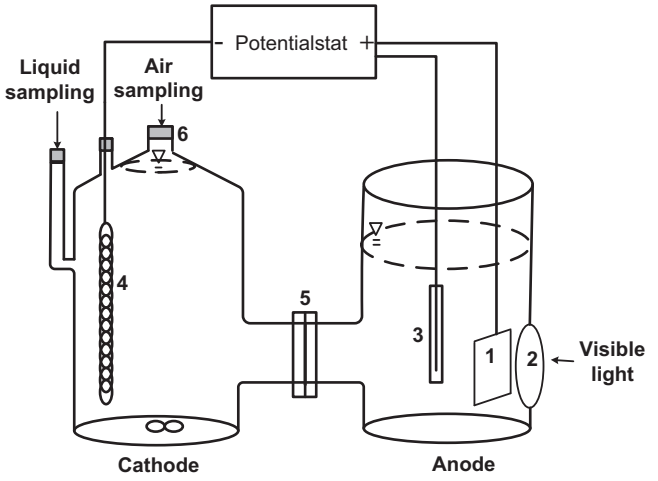

Fig. 1. Schematic diagram of photoelectrochemical system: (1) photoanode (N-doped TiO_2 thin film), (2) quartz window, (3) reference electrode (SCE), (4) counter electrode (copper wire), (5) cation exchange membrane and (6) septum.

(Sigma–Aldrich, USA) on an ITO coated glass (SPI Supplies Inc., PA, USA) was ablated with a KrF excimer laser (Lambda physic LPX 305, λ = 248 nm) under nitrogen and oxygen atmosphere. The apparatus setup was given by Lin et al. [29] in details. A mixture of N_2 and O_2 (4:1) was purged into the system, while the chamber pressure was maintained at 13.3 Pa. Two 500-W halogen lamps were used as irradiative heating source to control the substrate temperature up to 600 °C. The NTTF was characterized for microstructure and morphology with a scanning electron microscopy (SEM, JSM 7400F). The crystal structures of NTTF were characterized by X-ray diffraction (Rigaku D-Max B) with Cu Kα radiation (λ = 1.54 Å) operating at a voltage of 30 kV and a current of 30 mA. Samples were analyzed by Brag Brentano geometry in the range of 20 and 80°. UV–visible spectroscopy (PerkinElmer instruments, Lambda 750) was used to obtain the absorbance spectra of NTTF over a range of 300 and 800 nm. XPS spectra of N 1s, Ti 2p and C 1s regions were collected using X-ray photoelectron spectroscopy. XPS results show that the nitrogen content of the NTTF was 3% (by atomic weight).

A copper wire (Fisher Scientific, 155451A-16AWG-B16, od: 1 mm, length: 163 cm, total surface area: 51.2 cm^2), pretreated by alternatively polarizing at 10 V in 0.1 M of H_2SO_4 solution, was used as the counter electrode. The electrolytes were 0.1 M of NaCl and 0.1 M of $KHCO_3$ in the anodic and cathodic chamber, respectively. In the cathodic chamber, high purity carbon dioxide (99.999%) gas was bubbled into the $KHCO_3$ solution (0.1 M, pH 8.3) for 1.5 h at a rate of 10.8 mL s^{-1} until saturation solubility. The final solution had a pH of 6.8 and saturated CO_2 concentration of 0.13 M. A self-designed H-type reactor was made to separate the anode and cathode for purpose of concurrent MO degradation reaction. The two chambers were separated with a cation-exchange membrane. A quartz window (7 cm^2), on the side of the anodic chamber received the light irradiation. The potential for both current–potential measurement and PEC degradation experiments were controlled by a potentiostat (model AFRDE 4, Pine Instrument Inc., USA). A 100-W Xe lamp, that emitting monochromatic light at an average incident light intensity of 3.12 mW cm^{-2} (model RF-5301, Shimadzu, Japan) was used as the light source. Light intensity was measured by a high-sensitivity thermal sensor (model 3A-P-SH-V1, OPHIR, USA).

The gas and liquid samples were taken 5 times with the interval of 1 h during experiment. Table S1 lists the instrument used and experimental conditions for the photo-electrochemical reduction of CO_2.

2.3. Analytical methods

Hydrogen was analyzed using a gas chromatography system (HP 5890 Series II) with TCD detector (Packing: Alltech Hayesep D 100/120, Tubing: 1/8'' Nickel, Length: 20′, carrier gas: Helium at 30 mL/min, oven temperature: 35 °C, injection and detector temperature: 120 °C, and sample volume: 100 μL). Methanol and methane were analyzed using gas chromatography (HP 5890 Series II) with FID detector (Packing: SUPELCO Supel-Q PLOT, fused silica capillary column, 30 mm × 0.32 mm). The flow rate were 3, 32, 300 mL/min for helium carrier gas, air and hydrogen (fuel), respectively. For methanol analysis, the injection volume was 2 μL and the temperature setting for oven, injection, and detector were 50, 100, and 250 °C, respectively. For methane measurements, oven, injection, and detector temperatures were set as 50, 100, 250 °C, respectively. The injected volume for methane analysis was 1 mL for each sample.

For the liquid samples, formic acid, were analyzed using a Dionex ion chromatograph (IC) system which includes a GP50 pump, ED 40 conductance detector and automatic sampler (model As 40). The separation part was IonPac AC20 column (4 mm × 250 mm.) The flow rate of the mobile phase effluent, NaOH, was 1 mL/min and the injected volume was 200 μL for each formic analysis. Formaldehyde was analyzed high performance liquid chromatography (HPLC, Hewlett Packard series 1100). The liquid samples were derivatized with 2,4-dinitrophenylhydrazine with modification according to Lin et al. [32]. Briefly, dissolve 5 mg of DNPH in 40 mL solution which contains 12 M HCl, DI water, and acetonitrile with a volume ratio of 3.5:1:0.52. An aliquot of 1.5 μL the above reagent was then added into 1.5 mL of formaldehyde for derivatization. The final solutions were well-mixed to enable derivatization under ambient temperature. Formaldehyde-DNPH samples were measured by HPLC with a UV detector. The HPLC system was operated with binary gradients consisting of acetonitrile and H_2SO_4 (pH 3.0) with a flow rate of 1.0 mL/min. The separation component of HPLC was Varian Inertsil 5-μ ODS-2 column (150 mm × 4.6 mm) operating at ambient temperature. The injection volume was 60 μL for each sample.

The carbon dioxide concentration in the liquid phase was measured by flow injection analysis according to Jardim et al. [34]. H_2SO_4 (0.2 M; Fisher Scientific, USA) and deionized water were used as the mobile phase with the rate of 1.6 mL/min. In the process, 0.5 mL of the sample containing carbonate species, namely, CO_2, HCO_3^-, and CO_3^{2-}, were injected into a carrier fluid (DI water). Once the sample was brought in contact with the H_2SO_4 solution, carbon dioxide were produced under the acidic condition and diffused through a PTFE membrane. The diffused carbon dioxide was collected in the deionized water continuously while passing through a conductivity detector. The total carbon dioxide concentration in the sample was measured with increase in conductivity. Calibration curves in the range of 0.01–0.1 M of carbon dioxide were prepared using $KHCO_3$. The carbon dioxide concentration in the gas phase was measured with gas-chromatography (5890 Series II) with TCD detector (stock # 16166, Lot # 197, packing: Hayesep D 100/120, tubing: 1/8'' nickel, length: 20′, carrier gas: helium @ 30 mL min^{-1}, oven temperature: 35 °C, injection and detector temperature: 120 °C, and sample volume: 25 μL). The standard CO_2 gas with a purity of 99.98% was aspirated and injected into the GC-TCD system at volume of 1–100 mL using gas syringe. Methyl orange was analyzed with UV–vis spectrophotometry (HP 8452A diode array spectrophotometer) at a wavelength of 450 nm.

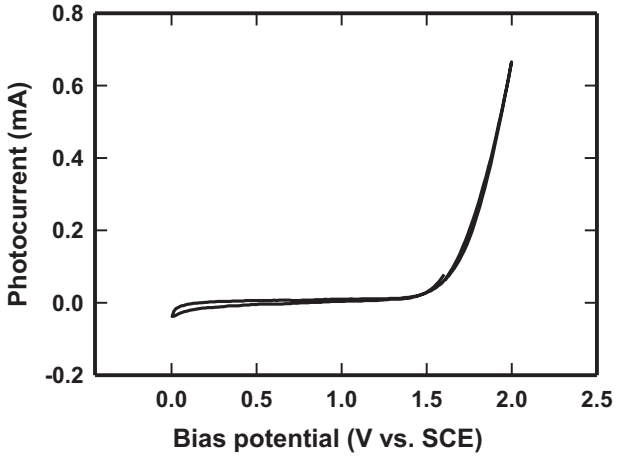

Fig. 2. Cyclic voltammetry scans in the presence of 1 ppm of MO and 0.1 M NaCl in the anodic chamber and 0.1 M $KHCO_3$ in the cathodic chamber. Experimental conditions: light source = 100-W Xe lamp (3.12 mW cm^{-2}); working electrode = NTTF; reference electrode = SCE; counter electrode = Cu.

3. Results and discussion

3.1. Current–potential curves of N-doped TiO_2 thin film

Fig. 2 illustrates the voltammetric behavior of a NTTF photoanode recorded at 50 mV s^{-1}. The current–potential curves were recorded at 298 K. In the anodic chamber, NTTF works as a photoanode with 1 ppm of MO as the anolyte. In general, the solution resistance is high between the working and the reference electrode, which would create significant IR drop, leading to the deformation of current–potential responses [35]. To overcome this high IR drop NaCl was added to the anolyte at a concentration of 0.1 M as to increase the conductivity. Meanwhile, in the cathodic chamber, a copper wire was used as cathode with solution containing $KHCO_3$ (0.1 M) saturated with CO_2. The applied voltage in this study started from 0 and ultimately went up to 2 V in order to manipulate the electrons generation at the photoanode (i.e. working electrode) which was in contrast to most related studies where anodic reaction was not the focus. Therefore, as a positive bias potential is applied in this tri-electrode PEC system, the electrons would be transferred from the working electrode to the counter electrode.

Fig. 2 shows that the total current took off abruptly at potential of ca. 1.5 V (vs. SCE). Ohta et al. [36] investigated the photoelectrochemical reduction of CO_2 in methanol solution using various metallic electrodes including Ti, Co, Pt, Zn, Au, Fe, Ni, Sn, and Ag, in CO_2 and reported that Ti had the highest onset potential of 1.6 V (vs. SCE), which is similar to that of NTTF in this study. The current was generated from direct electrochemical oxidation of MO before the bias potential reached 1.5 V (vs. SCE). When the applied bias potential exceeded the onset potential, the anodic current increased greatly with applied potential, which might result from electrochemical oxidation of MO in addition to oxygen evolution, i.e., $2H_2O \rightarrow 4H^+ + O_2 + 4e$. Beyond the onset potential, the total current reached the maximum value of ca. 0.65 mA at 2 V (vs. SCE). This indicated that the photocurrent generated at the NTTF photoanode could be effectively transferred to the counter electrode by this positive potential, which would be beneficial to the separation of photo-generated holes and electrons. In other words, the greater the applied bias potential, the greater extent the decrease in electron–hole recombination (Table S2). Furthermore, greater external potential applied the greater the degree of electrochemical oxidation reaction in anodic chamber will be. Zhao and Zhu [37] have showed that PCE can effectively degrade aqueous pollutants by the synergetic effect of electro-oxidation and photocatalysis.

Table 1
Faradaic efficiency (%) of CO_2 reduction and its products (in 0.1 M $KHCO_3$ electrolyte).

Time (h)	HCOOH (%)	HCOH (%)	CH_3OH (%)	CH_4 (%)	H_2 (%)	Total (%)
1	5.01	1.04	5.41	0.00	0.00	11.46
2	4.44	0.69	5.02	2.00	10.90	23.05
3	4.52	0.48	4.48	2.26	14.11	25.85
4	3.30	0.46	3.43	6.35	26.15	39.69
5	2.60	0.39	3.26	7.83	50.34	64.42

3.2. Faradaic efficiency

Table 1 gives the Faradaic efficiencies of photoelectrochemical CO_2 reduction with respect to by-products formed. We have detected the formation of four products, namely, formic acid, formaldehyde, methanol, and methane from CO_2 reduction and hydrogen from water splitting. The photocurrent was 0.4 (±0.1) mA at the bias potential of 2 V (vs. SCE) under 100-W irradiation (Xe lamp, 3.12 mW cm^{-2}). The highest Faradaic efficiency was 5.01, 1.04, 5.41, and 7.83% for HCOOH, HCOH, CH_3OH and CH_4, respectively. Interestingly Faradaic efficiency decreased with reaction time for HCOOH, HCOH and CH_3OH but CH_4 and H_2. Hydrogen reached the highest Faradaic efficiency of 50.34% at the fifth hour. It is hypothesized that CO_2 reduction takes place as the carbon oxidation state changes from +IV (CO_2) to +II (e.g., HCOOH), 0 (e.g., HCOH), −II (e.g., CH_3OH) and then −IV (e.g., CH_4). The following in-series reaction is proposed (Eq. (1)):

$$CO_2 \xrightarrow{k_1} HCOOH \xrightarrow{K_2} HCOH \xrightarrow{k_3} CH_3OH \xrightarrow{k_4} CH_4 \quad (1)$$

Therefore, as CO_2 is reduced continuously in the system, the final product of CH_4 increases concomitantly. H_2 formation had the highest Faradaic efficiency in our CO_2 reduction system after the second hour. Previous related CO_2 reduction studies indicated that hydrogen formation contributed to a certain part of Faradaic efficiency [13,16,20,36]. However, hydrogen formation is a disadvantage as far as the yield of CO_2 reduction products is concerned, although hydrogen is useful form of energy. The issue of high hydrogen formation will be discussed in the following section.

Table 2 summarizes the formation of CO_2 reduction by EC [5–7,33,34], PC [11,50] and PEC [7,20,22] using various electrodes and electrolytes. Major products such as CO, HCOOH, CH_3OH, CH_4, C_2H_4 and H_2 have been reported. Results also show that the Faradaic efficiency differs among various species and experimental conditions such as temperature, light intensity, electrolyte, and electrode material. For examples, Koci et al. [16] studied CO_2 reduction using Ag doped-TiO_2 and reported the product yield in the following order: $CH_3OH > CH_4 > CO > H_2$. Ohta et al. [36] studied the electrochemical reduction of CO_2 using nine high purity metallic electrodes and reported that methane and hydrogen evolution on each of nine electrodes with Faradaic efficiency in the range of 0.2–2.7% and 4.4–114%, respectively. Kaneco et al. [5,6] investigated electrochemical CO_2 reduction in CsOH/MeOH and KOH/MeOH electrolyte using copper electrode at low temperature of 243 K and reported ethylene as major product. Le et al. [7] demonstrated that cuprous oxide electrodes were remarkably better than air-oxidized or anodized Cu electrodes in CO_2 reduction suggesting that Cu (I) species may play a critical role in selectivity to CH_3OH.

3.3. Effect of CO_2 solubility

Methanol is a better solvent for CO_2 than water, particularly at low temperature. The solubility of CO_2 in methanol is about four and eight times that in water at ambient temperature and at temperatures below 273 K, respectively. Therefore, methanol has been used as an absorbent of carbon dioxide in the Rectisol process at 243–263 K [38]. It is conceivable that higher soluble CO_2 concentrations accompanies higher yield of CO_2 reduction products. However, to the best of our knowledge, there is no report about the effect of initial CO_2 concentration on the CO_2 reduction in two-chamber PEC system using NTTF photoanode. CO_2 reduction experiment was conducted in three concentrations of methanol, i.e., 0, 20, and 40%. All cathodic electrolytes were bubbled with CO_2 gas at 99.99% purity for 90 min before experiments.

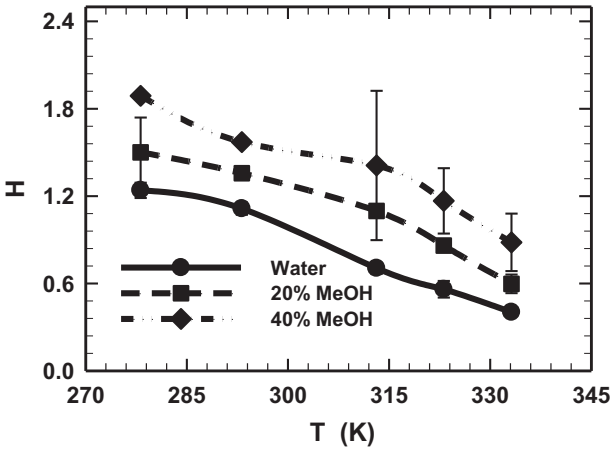

Fig. 3. Henry's Law constant carbon dioxide (M/atm) as a function of methanol concentration and temperature.

Fig. 3 shows the Henry's constants (dimensionless) of CO_2, $H(CO_2)$, as a function of temperature (278, 293, 313, 323 and 333 K) for solutions containing 0, 20 and 40% of methanol. The CO_2 solubility increases with increasing methanol concentration that agrees with previous studies. At room temperature (293 K), the $H(CO_2)$ value was 1.11, 1.37, and 1.57 for solutions containing 0, 20 and 40% of methanol, respectively. Fig. 3 also demonstrates that the CO_2 solubility increases with the decreased temperature. For 40% methanol, the $H(CO_2)$ was 1.79, 1.53, 1.46, 1.25, and 0.98 for 278, 293, 313, 323, and 333 K, respectively. Xia et al. [39] examined the solubility of carbon dioxide in mixtures of water and methanol at various methanol mole fractions (0.05, 0.10, 0.25, 0.50, 0.75, 0.90, 0.95, and 1.00), temperatures (313.75, 354.35, and 395.0 K), and total pressures (p) up to about 10 MPa and reported that the solubility of carbon dioxide was significantly higher in the methanol-rich than the water-rich solutions.

Fig. 4 illustrates the influence of CO_2 solubility on the yield of HCOOH, HCOH, CH_4 and H_2. Notably, CH_3OH was not measurable due to the high CH_3OH background concentration. The trends of CO_2 reduction products for three different concentrations of methanol-based electrolytes were similar. The concentration of both HCOOH and HCOH reached plateau whereas CH_4 and H_2 continued to increase in concentration. Furthermore, methane formation took place immediately in the presence of methanol whereas a lag in methane production was observed in solution in the absence of methanol. This might be due to direct CH_4 formation from CH_3OH (see Eqs. (2.13) and (2.14) in Section 3.4) in the methanol-based electrolyte. From Fig. 4(a)–(c), the yield of formic acid, formaldehyde and methane in methanol (40%)-based electrolyte were ca. 12, 3, and 2.7 times higher than that in the methane free (0%) electrolyte. Results demonstrate clearly that higher dissolved CO_2 concentrations can enhance the formation of CO_2 reduction products. Fig. 4(d) shows hydrogen formation decreases with increasing methanol concentration in the electrolyte. Hydrogen appeared in the second reaction hour in water-based electrolyte, but was not detectable until the fourth reaction hour in methanol-based electrolyte. Results indicated

Table 2
Summary of CO_2 reduction by EC, PC and PEC.

Method	Products	Applied voltage	Temperature (K)	Cell	Electrolyte	CO_2 bubbled	Light source	Electrode	Reference
EC	CH_4: 1.3%[a] C_2H_4: 0.2%[a] CO: 0.2%[a] H_2: 86%[a]	−1.2 V vs. SCE	288 ± 0.5	H-type	0.01 M Benalkonzum chloride in MeOH	Y	N.A.	Fe	Ohta (1998) [34]
EC	C_2H_4: 32.3% [a] CH_4: 8.3%[a]	−4.0 V vs. Ag/Ag/Cl	243 ± 0.5	H-type	CsOH/MeOH	Y	N.A	Cu	Kaneco (1999) [5]
PC	CH_3OH: 10%[b]	N.A.	N.A.	Single	0.2 N NaOH	Y	8 W Hg lamp	Cu/TiO_2	Tseng (2002) [11]
EC	CH_3OH: 60.5%[a]	−0.8 V vs. SCE	Room temperature	H-type	0.5 M $NaHCO_3$	Y	N.A.	RuO_2/TiO_2 nanotubes modified Pt electrode	Qu (2005) [33]
EC	C_2H_4: 37.5%[a]	−4.0 V vs. Ag/Ag/Cl	243 ± 0.5	H-type	Saturated KCl in KOH/MeOH	Y	N.A.	Cu	Kaneco (2006) [6]
PEC	CH_4: 0.56%[a] C_2H_4: 0.8%[a]	−2.5 V vs. Ag/AgCl	258	H-type	0.1 N NaOH in methoanl	Y	500 W Xe lamp	p-InP	Kaneco (2009) [20]
PC	CH_3OH: 0.19[c] H_2: 0.015[c] CH_4: 0.85[c] CO: 0.05[c]	N.A.	N.A.	Single	Water saturated with CO_2	Y	8 W Hg lamp	7% Ag-TiO_2	Koci (2010) [50]
PEC	HCOOH: 62.3%[a]	−0.6 V vs. Ag/AgCl	N.A.	Single	Water	Y	Xe lamp	p-InP-Zn modified with ruthenium-complex polymer	Aria (2010) [22]
EC	CH_3OH: 38%[a]	−1.55 V vs. SCE	298 K	Single	0.5 M $KHCO_3$	Y	N.A.	Cu	Le et al. (2011) [7]
PEC	HCOOH: 5.01%[a] HCOH: 1.04%[a] CH_3OH: 5.41%[a] CH_4: 7.83%[a] H_2: 50.34%[a]	2 V vs. SCE	298 K	H-type	0.1 M$KHCO_3$	Y	100 W Xe lamp	Cu	This study

[a] Faradaic efficiency (%)
[b] Quantum efficiency (%)
[c] μmol/g-catalyst

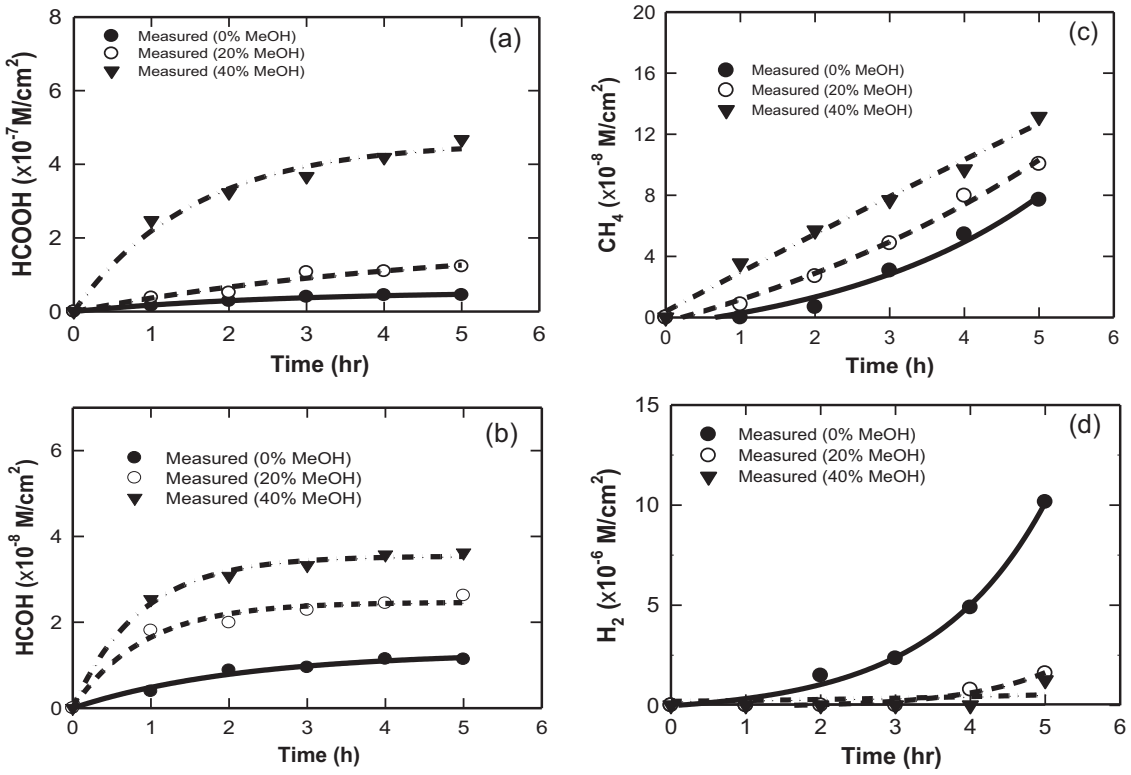

Fig. 4. The effect of the methanol concentration on photoelectrochemical reduction of CO_2 and its products, (a) HCOOH, (b) HCOH, (c) CH_4, and (d) H_2. Lines are predicted based on simulated first-order model, dots are experimental data. Experimental conditions: working electrode = NTTF; reference electrode = SCE; counter electrode = Cu; anolyte = 0.1 M NaCl + 0.1 M MO; catholyte = 0.1 M$KHCO_3$ in the presence of methanol at concentration from 0 to 40%; pH 6.0 (anode); pH 6.8 (cathode); temperature = 298 K and light source = Xe lamp (3.12 W cm^{-2}).

competition between hydrogen formation (water splitting) and CO_2 reduction reaction. Kaneco et al. [5] studied the electrochemical reduction of CO_2 in CsOH/methanol electrolyte on a Cu electrode and reported that the current efficiency for hydrogen formation at 243 K in CsOH/methanol electrolyte was suppressed to below 23% [5]. As shown in Fig. 4, the presence of methanol enhanced the production of formaldehyde, methane, and formic acid (in decreasing order) and the decrease in hydrogen. While it is thermodynamically possible to reduce methanol directly to methane, results appeared to demonstrate that the significant increase in the formation of reduction by-products was brought mostly from increase in CO_2 solubility as evident of the 10-fold increase in formaldehyde with respect to methane and formic acid. Generally, hydrogen formation comes from the electrochemical reduction of H_2O. Thus, methanol-based electrolyte might suppress the hydrogen formation due to the decreasing water fraction in methanol-based electrolyte.

Fig. 5 shows the hydrogen formation as a function of H_2O mole fraction. H_2O mole fraction of 1, 0.91 and 0.77 is corresponding to 0, 20 and 40% methanol concentration in the electrolyte, respectively. Hydrogen formation increases with increasing reaction time owing to enhanced water reduction reaction as more electrons are available in the system. Obviously, lower H_2O mole fraction in the electrolyte aids in suppressing hydrogen formation. The suppression of hydrogen formation is important as not to waste electrons on hydrogen evolution but on promoting CO_2 reduction. Therefore, methanol-based electrolyte not only increases CO_2 solubility but also impedes hydrogen formation due in part to decrease in H_2O mole fraction.

3.4. Preliminarily proposed CO_2 reduction mechanism

Photo-generated electrons and holes are formed on the surface of NTTF with sufficient photonic energy and appropriate wavelength. However, the electrons and holes that are formed upon solar light irradiation will undergo rapid recombination, estimated at a rate of $(3.2 \pm 1.4) \times 10^{-1}$ cm^3 s^{-1} [40]. Hole–electron recombination will decrease the overall photocatalysis quantum yield. Moreover, since holes are strong oxidant, they will tend to oxidize photocatalytic products such as methanol or organic acids back to CO2. Therefore, the PEC process, a combination of electrooxidation and photocatalysis, minimizes the hole–electron recombination and to enables the separation of electrons and holes by applying

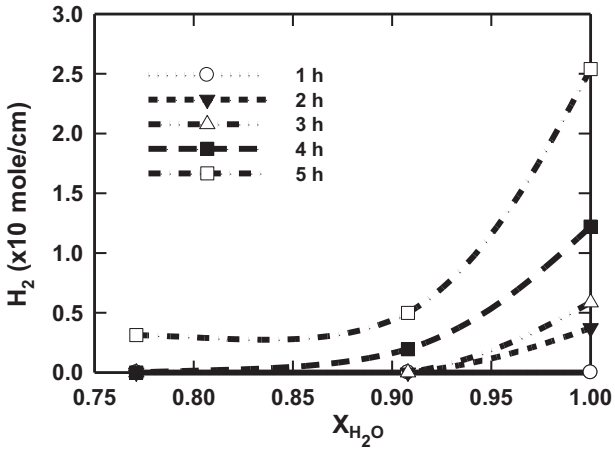

Fig. 5. Hydrogen generation as a function of H_2O mole fraction in the electrolyte. Experimental conditions: working electrode = NTTF; reference electrode = SCE; counter electrode = Cu; anolyte = 0.1 M NaCl + 0.1 M MO; catholyte = 0.1 M$KHCO_3$ in the presence of methanol at concentration from 0 to 40%; pH 6.0 (anode); pH 6.8 (cathode); temperature = 298 K; light source = Xe lamp (3.12 W cm^{-2}) and $x_{H_2O} = n_{H_2O}/(n_{H_2O} + n_{MeOH})$.

a bias potential between the anode and the cathode. At the anode, holes and electrons were generated when the NTTF was excited by an appropriate visible light (Eq. (2.1)), i.e.,p̂

$$\text{NTTF} + h\nu \rightarrow h^+ + e^- \quad (2.1)$$

The holes first react with water molecules that are absorbed on the NTTF surface, resulting in the production of hydroxyl radicals and hydrogen ions (Eq. (2.2)), i.e.,

$$h^+ + H_2O(\text{ads}) \rightarrow OH^\bullet + H^+ \quad (2.2)$$

As the bias potential was applied, the adsorbed water molecule at the anode was oxidized to oxygen according to the following reaction (Eq. (2.3)), i.e.,

$$2H_2O(\text{ads}) \rightarrow O_2 + 4e^- + 4H^+ \quad (2.3)$$

Notably, the electrons generated at the anode are driven to the cathode by a potentiostat, i.e., electron pump. Hydroxyl radical and oxygen play important role in the oxidation reaction in the anodic chamber. The hydroxyl radical (E^o = 2.72 V), a strong oxidant plays an important role in the degradation of organic contaminants in the photo-anodic chamber. The proton ions will pass through the cation exchange membrane to the cathodic chamber where it is reduced to hydroxyl radical (Eq. (2.5)). At the cathode, the electrolysis of water leads to formation of hydrogen radicals ($H^\bullet$) and OH^- (Eq. (2.4)), i.e.,

$$H_2O + e^- \rightarrow H^\bullet + OH^- \quad (2.4)$$

In the absence of dissolved oxygen, proton will be reduced to hydrogen radical (Eq. (2.5)), i.e.,

$$H^+ + e^- \rightarrow H^\bullet \quad (2.5)$$

The hydrogen radical will then recombine rapidly to form hydrogen molecule (Eq. (2.6)), i.e.

$$H^\bullet + H^\bullet = H_2 \quad (2.6)$$

Water splitting reaction for hydrogen formation using PEC has been studied [41–45]. Most importantly, hydrogen radical, a strong reductant, consequently contributes to the formation of various CO_2 reduction products, namely, formic acid (HCOOH), formaldehyde (HCOH), methanol (CH_3OH), and methane (CH_4). (Eqs. (2.7)–(2.14)) [19,29,46]. Intuitively, the first CO_2 reduction product would be formic acid radical, $HCO_2^\bullet$, which has a carbon oxidation number of III.

$$CO_2 + H^\bullet \rightarrow HCO_2^\bullet \quad (2.7)$$

Formic acid radical is not stable; it will undergo further interaction with hydrogen radical to form formic acid (HCOOH), which carbon oxidation number is II.

$$CHO_2^\bullet + H^\bullet \rightarrow HCOOH \quad (2.8)$$

Continuing interaction between formic acid with hydrogen radical yields formaldehyde radical, $CH_3O_2^\bullet$, which carbon oxidation number is I, i.e.,

$$HCOOH + H^\bullet \rightarrow CH_3O_2^\bullet \quad (2.9)$$

Reaction between formaldehyde radical and hydrogen radical converts the former to formaldehyde (CH_2O) which carbon oxidation state is 0.

$$CH_3O_2^\bullet + H^\bullet \rightarrow CH_2O + H_2O \quad (2.10)$$

Reaction between formaldehyde and hydrogen radical yields methanol radical, $CH_3O^\bullet$, which carbon oxidation number is –I, i.e.,

$$CH_2O + H^\bullet \rightarrow CH_3O^\bullet \quad (2.11)$$

Attack on the methanol radical by hydrogen radial converts the former to methanol (CH_3OH), which carbon oxidation number is –II, i.e.,

$$CH_3^\bullet + H^\bullet \rightarrow CH_3OH \quad (2.12)$$

Reaction between methanol and hydrogen radical forms methyl radical, $CH_3^\bullet$, which has a carbon oxidation number of–III, i.e.,

$$CH_3OH + H^\bullet \rightarrow CH_3^\bullet + H_2O \quad (2.13)$$

Finally, interaction between methyl radical and hydrogen radical converts the former to methane (CH_4).

$$CH_3^\bullet + H^\bullet \rightarrow CH_4 \quad (2.14)$$

Furthermore, there were several CO_2 reduction studies detailing the mechanism of the formation of byproducts and reported that methanol was directly derived from CO_2 species. Naitoh et al. [47] studied the reduction of deuterium-labeled methanol and reported that none of the above CO_2 reduction products was derived from methanol. Kaneco studied CO_2 reduction in methanol electrolyte and reported results similar to that of Naitoh et al. [5,6,20,23,48–51]. Yui et al. [52] studied photocatalytic reduction of CO_2 using Pd-TiO_2 as photocatalyst and found that methane was produced directly from $^{13}CO_2$ based on the m/e = 17 which was attributed to $^{13}CH_4$ under $^{13}CO_2$ atmosphere. Their results agreed with the findings of Dimitrijevic et al. [53] who reported that the carbonate species were source of the photocatalytic CH_4 formation.

Another possible pathway of CO_2 reduction would be: $CO_2 \rightarrow CO \rightarrow C \rightarrow CH_2 \rightarrow CH_4$ to yield the end product of CH_4 through different intermediates. This has been proposed based on the Rectisol process and also on electrolytic reduction of CO_2 [20,38,54]. In the present study, no CO was observed, however.

3.5. Rate constants

According to the above reaction scheme, aqueous CO_2 reacts with hydrogen radical to form formic acid (Eq. (2.8)), formaldehyde (Eq. (2.10)), methanol (Eq. (2.12)) and methane (Eq. (2.14)) in series. The intermediates (Eqs. (2.7), (2.9), (2.11) and (2.13)) generated in each step are steady state species that are not stable. The CO_2 reduction process can be described by a series of individual first-order reactions, namely,

$$\frac{d[CO_2]}{dt} = -k_1[CO_2] \quad (3.1)$$

$$\frac{d[HCOOH]}{dt} = k_1[CO_2] - k_2[HCOOH] \quad (3.2)$$

$$\frac{d[HCOH]}{dt} = k_2[HCOOH] - k_3[HCOH] \quad (3.3)$$

$$\frac{d[CH_3OH]}{dt} = k_3[HCOH] - k_4[CH_3OH] \quad (3.4)$$

$$\frac{d[CH_4]}{dt} = k_4[CH_3OH] \quad (3.5)$$

where t is reaction time and k_1, k_2, k_3, and k_4 are the reaction rate constants of CO_2, HCOOH, HCOH, and CH_3OH, respectively.

Because Eqs. (3.1)–(3.5) are sequential, they can be solved as follows with the following initial condition, $[HCOOH]_o = [HCOH]_o = [CH_3OH]_o = 0$.

$$[CO_2] = [CO_2]_o e^{-k_1 t} \quad (3.6)$$

$$[HCOOH] = \frac{k_1[CO_2]_o}{k_2 - k_1}\left(e^{-k^1 t} - e^{-k^2 t}\right) \quad (3.7)$$

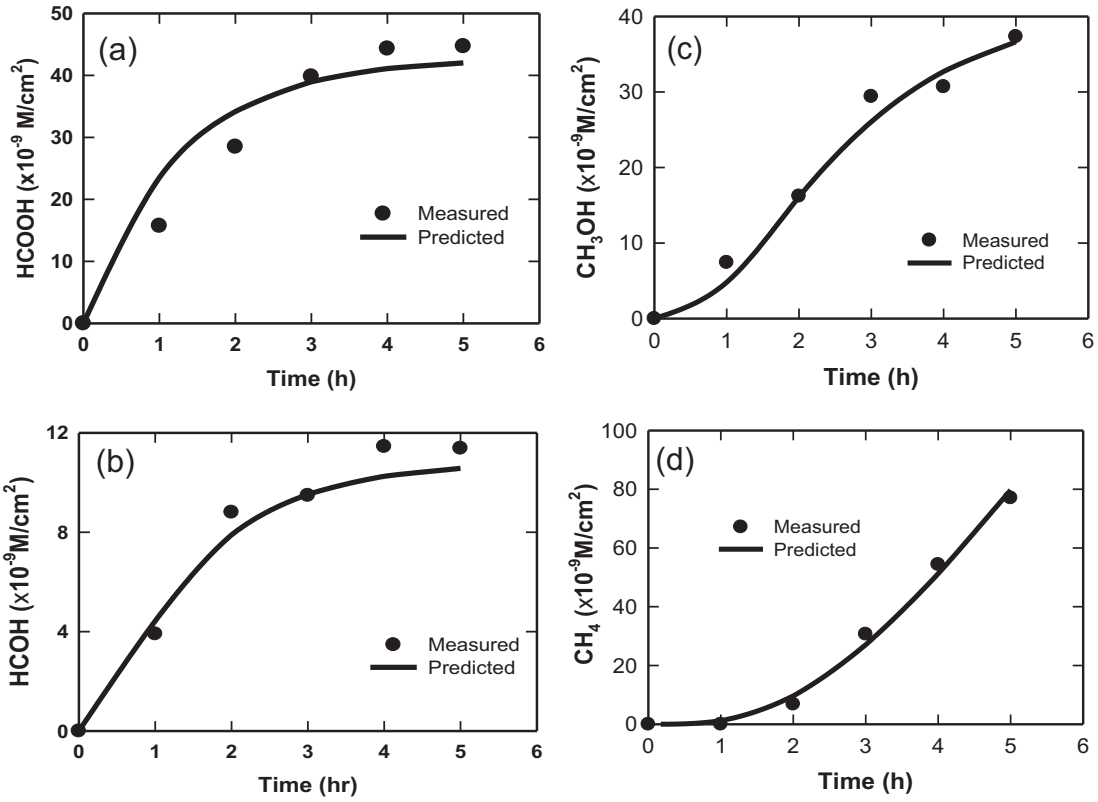

Fig. 6. Comparison of experimental data with predicted concentrations for (a) HCOOH, (b) HCOH, (c) CH_3OH, and (d) CH_4 based on differential first-order models. Experimental conditions: working electrode = NTTF; reference electrode = SCE; counter electrode = Cu; anolyte = 0.1 M NaCl + 0.1 M MO; catholyte = 0.1 M$KHCO_3$ in the presence of methanol at concentration from 0 to 40%; pH = 6.8 (cathode); temperature = 298 K and light source = Xe lamp (3.12 W cm^{-2}).

$$[\mathrm{HCOH}] = \frac{k_1 k_2 [\mathrm{CO_2}]_o}{k_3 - k_2}\left(\frac{e^{-k_1 t} - e^{-k_2 t}}{k_2 - k_1} - \frac{e^{-k_1 t} - e^{-k_3 t}}{k_3 - k_1}\right) \tag{3.8}$$

$$[\mathrm{CH_3OH}] = \frac{k_1 k_2 k_3 [\mathrm{CO_2}]_o}{(k_2 - k_1)(k_3 - k_1)}\left(\frac{e^{-k_1 t} - e^{-k_4 t}}{k_4 - k_1} - \frac{e^{-k_3 t} - e^{-k_4 t}}{k_4 - k_3}\right) - \frac{k_1 k_2 k_3 [\mathrm{CO_2}]_o}{(k_2 - k_1)(k_3 - k_2)}\left(\frac{e^{-k_2 t} - e^{-k_4 t}}{k_4 - k_2} - \frac{e^{-k_3 t} - e^{-k_4 t}}{k_4 - k_3}\right) \tag{3.9}$$

$$[CH_4] = k_1 k_2 k_3 [CO_2]_o \left(\frac{e^{-k_1 t} - e^{-k_2 t}}{(k_4 - k_3)(k_3 - k_2)(k_2 - k_1)} - \frac{e^{-k_1 t} - e^{-k_3 t}}{(k_4 - k_3)(k_3 - k_2)(k_3 - k_1)} - \frac{e^{-k_1 t} - e^{-k_2 t}}{(k_4 - k_3)(k_4 - k_2)(k_2 - k_1)} + \frac{e^{-k_1 t} - e^{-k_4 t}}{(k_4 - k_3)(k_4 - k_2)(k_4 - k_1)} + \frac{e^{-k_1 t} - e^{-k_2 t}}{k_3 (k_3 - k_2)(k_2 - k_1)} - \frac{e^{-k_1 t} - e^{-k_3 t}}{k_3 (k_3 - k_2)(k_3 - k_1)} + \frac{e^{-k_1 t} - e^{-k_2 t}}{k_3 k_2 (k_2 - k_1)} + \frac{e^{-k_1 t} - 1}{k_1 k_2 k_3}\right) \tag{3.10}$$

Fig. 6 compares the experimental and the simulated results for CO_2 reduction and its products. The electrolyte contained 1 mg/L of methyl orange and 0.1 M of NaCl to maintain the conductivity in the anodic chamber. Meanwhile, the catholyte was made of 0.1 M $KHCO_3$ (initial pH 8.3) bubbled with CO_2 gas until saturation (pH 6.8). The pH value of the catholyte remained constant at ca. 7.3–7.4 throughout the entire experiment. The photocurrent was 0.5 mA from the NTTF photoanode under illumination, at a 2.0 V bias potential. Formic acid, formaldehyde and methanol were detected in liquid phase while methane was detected in gas phase. Results in Fig. 6(a)–(c) illustrate that the measured HCOOH, HCOH and CH_3OH concentrations increased apparently in the first three hours and then reached a constant value after the fourth hour. However, the measured CH_4 increased continuously from the second hour, as shown in Fig. 6(d). The measured values agreed well with simulated results for HCOOH, HCOH, CH_3OH and CH_4. The performance of the model was obtained relative to the measurements using the index of agreement (IOA) [55,56],

$$d_1 = 1 - \frac{\sum_{i=1}^{N} \left|P_i - O_i\right|}{\sum_{i=1}^{N} \left|P_i - \overline{O}\right| + \left|O_i - \overline{O}\right|} \tag{4}$$

where d_1 stands for IOA, P_i and O_i are the predicted and measured values, respectively, with a sample size of N, and $\overline{O}$ is the average of all measured data. Table 3 summarizes the statistical

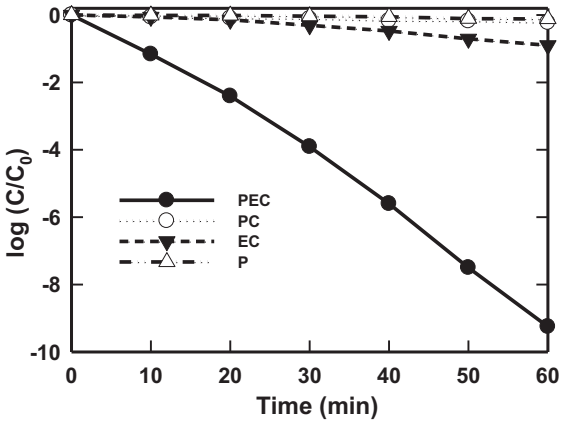

Fig. 7. Comparing the treatment of MO by PEC, PC, EC, and P methods. Experimental conditions: initial concentration of MO = 1 ppm; light source = 3.12 mW cm^{-2} (100 W Xe lamp); working electrode = NTTF; reference electrode = SCE; counter electrode = Cu; bias potential = 2 V (vs. SCE); pH 6.0 (anode); pH 6.8 (cathode); electrolyte = 1 ppm MO in 0.1 M NaCl (anode); electrolyte = 0.1 M $KHCO_3$ (cathode) and temperature = 298 K.

data for the comparison of measured and simulated HCOOH, HCOH, CH_3OH and CH_4. The agreement between prediction and measurement is regarded as good when IOA exceeds 0.5 [56]. The rate constants were calculated as 6.68×10^{-7}, 2.18×10^{-4}, 8.62×10^{-4} and 2.27×10^{-4} (s^{-1}), for k_1, k_2, k_3, and k_4 respectively. Notably, k_1 is thousand times smaller than the others due to the relatively high initial carbon dioxide concentration (0.13 M) in the cathodic chamber.

3.6. Concurrent oxidation of methyl orange

The effectiveness of the present PEC process was assessed further by studying the concurrent oxidation of methyl orange (MO) at the photoanode. The degradation of MO by PEC was compared with that of photocatalytic (PC), electrochemical (EC) and direct photolysis (P) processes. Fig. S1 shows that the dominant absorption wavelength of MO was around 455 nm. The PEC, PC and photolysis experiments were examined under illumination of 100-W Xe lamp at 3.12 mW cm^{-2} energy. Applied voltage in the PEC and the EC process was 2.0 V (vs. SCE), the best response of photocurrent-bias potential based on CV results showed above (Fig. 2). Fig. 7 shows a plot of $\log(C/C_0)$ versus reaction time. It was clear that PEC gave the best MO degradation due to the combined reaction of electrochemical oxidation and photocatalysis. Upon the application of bias potential, the photocatalytic degradation of MO was enhanced by the timely separation and transfer of photogenerated electrons and holes. The action enhanced not only the electrochemical but also the photocatalytic oxidation. Based on results in Fig. 7, the degradation rate constants were estimated as 6.9×10^{-5}, 1.57×10^{-4}, 3.50×10^{-4} and 4.48×10^{-3} s^{-1} for P, EC, PC and PEC processes, respectively. The PEC process was able to achieve a 10-log degradation of MO versus less than 1-log by all other methods studied. Zhang et al. [57] and Peng et al. [58] reported rate constant of 1.63×10^{-4} and 4.28×10^{-4} s^{-1} for photocatalytic degradation of MO using TiO_2 film and N-doped titanium nanotubes respectively. The applied voltage in PEC method is a key point regarding the degradation efficiency. As the applied bias potential was below the redox potential of the target compounds, the increasing bias potential could increase the photocatalytic ability by promoting the separation and transfer of photogenerated holes and electrons. In contrast, the applied bias potential, beyond the redox potential of target compounds, not only can separate the holes and electrons but also can directly electrolyze target compounds [37]. From the CV results (Fig. 2), it is seen that when the bias potential exceeded 1.6 V, the current increased significantly due to the electro-oxidation of MO and oxygen evolution. In a two-chamber PEC system, applying potentials greater than the NTTF flat band potential under illumination condition could transfer the photogenerated current to an external circuit and arrive at the cathode. This may increase the photogenerated active species on the surface of photoanode by decreasing the recombination rate of photogenerated holes and electrons.

Table 3
The rate constant (k, s^{-1}) of photoelectrochemical reduction of CO_2 at Cu electrode in $KHCO_3$ (0.1 M) electrolyte.

	Rate constant (1/s)	IOA
k_1	6.68×10^{-7}	0.87
k_2	2.18×10^{-4}	0.92
k_3	8.62×10^{-4}	0.94
k_4	2.27×10^{-4}	0.96

Catholyte: $KHCO_3$ (0.1 M), anolyte: NaCl (0.1 M), temperature 298.15 K, potential 2.0 V (vs. SCE).

4. Conclusion

Simultaneously photoelectrochemical reduction of CO_2 and oxidation of methyl orange takes place in a PEC system where electrons and holes were separated by an external applied bias potential upon the irradiation of a novel photoanode, nitrogen-doped TiO_2 thin film. The successful separation of photo-generated electrons and holes minimizes their recombination, thereby drastically improves the overall photocatalytic efficiency. The NTTF provides a total current of 0.65 mA at 2 V vs. SCE upon illumination under a 100 W-Xe lamp. The highest Faradaic efficiency of CO_2 reduction products was 5.01, 1.04, 5.41, and 7.83% for formic acid (HCOOH), formaldehyde (HCOH), methanol (CH_3OH) and methane (CH_4), respectively. The CO_2 solubility was increased by the addition of methanol (20 and 40% in the cathodic chamber) that resulted in increase in CO_2 reduction measured by increase in the amounts of all byproducts; there was a noteworthy increase in the concentration of formaldehyde by an order of magnitude greater than that of formic acid and methane. Results showed that methanol-containing electrolyte suppressed hydrogen generation. Preliminarily mechanism for the reduction of CO_2 was proposed. CO_2 reduction takes place following a sequential reaction according to which the oxidation state of carbon decreases from +IV (of CO_2), to +II (of formic acid), to 0 (of formaldehyde), to −II (of methanol), and then to −IV (of methane). Reaction was modeled by in-series first-order reaction. The index of agreement between observed and model predicted was in the range of 87 and 96%, which is significant. The photocatalytic oxidation efficiency of the PEC process was compared with other methods, namely, photocatalytic (PC), electrochemical (EC) and photolysis (P) by studying the degradation of hazardous chemicals exemplified by methyl orange. Results clearly showed the excellent performance of the PEC process capable of achieving a 10-log versus less than 1-log degradation of methyl orange by all other processes studied. Overall, the PEC process enables significant increase in photocatalytic capability in terms of chemical reduction of CO_2 and degradation of hazardous chemicals.

Acknowledgment

The senior author was supported by a grant, NSC9829171564109, from the National Science Council, Taiwan. We also wish to thank Professor J. H. Choi of Kongju National University, Korea, for valuable comments on the CV plot.

Appendix A. Supplementary data

Supplementary data associated with this article can be found, in the online version, at http://dx.doi.org/10.1016/j.apcatb.2012.04.037.

References

[1] G. Centi, S. Perathoner, Catalysis Today 148 (2009) 191–205.
[2] P. Usubharatana, D. McMartin, A. Veawab, P. Tontiwachwuthikul, Industrial & Engineering Chemistry Research 45 (2006) 2558–2568.
[3] A.J. Bard, R. Parson, J. Jordan, New York and Basel, Marcel Dekker, Inc., 1985.
[4] Y. Hori, A. Murata, R. Takahashi, Journal of the Chemical Society, Faraday Transactions 1 (85) (1989) 2309–2326.
[5] S. Kaneco, K. Iiba, N. Hiei, K. Ohta, T. Mizuno, T. Suzuki, Electrochimica Acta 44 (1999) 4701–4706.
[6] S. Kaneco, H. Katsumata, T. Suzuki, K. Ohta, Electrochimica Acta 51 (2006) 3316–3321.
[7] M. Le, M. Ren, Z. Zhang, P.T. Sprunger, R.L. Kurtz, J.C. Flake, Journal of The Electrochemical Society 158 (2011) E45–E49.
[8] N.V. Rees, R.G. Compton, Energy & Environmental Science 4 (2011) 403–408.
[9] Y. Hori, K. Kikuchi, A. Murata, S. Suzuki, Chemistry Letters (1986) 897–898.
[10] Y. Hori, I. Takahashi, O. Koga, N. Hoshi, Journal of Physical Chemistry B 106 (2002) 15–17.
[11] I.H. Tseng, W.-C. Chang, J.C.S. Wu, Applied Catalysis B: Environmental 37 (2002) 37–48.
[12] Y. Ku, W.-H. Lee, W.-Y. Wang, Journal of Molecular Catalysis A: Chemical 212 (2004) 191–196.
[13] C.C. Lo, C.H. Hung, C.S. Yuan, J.F. Wu, Solar Energy Materials and Solar Cells 91 (2007) 1765–1774.
[14] S.S. Tan, L. Zou, E. Hu, Catalysis Today 131 (2008) 125–129.
[15] Z.Y. Wang, H.C. Chou, J.C.S. Wu, D.P. Tsai, G. Mul, Applied Catalysis A: General 380 (2010) 172–177.
[16] K. Koci, K. Mateju, L. Obalova, S. Krejcikova, Z. Lacny, D. Placha, L. Capek, A. Hospodkova, O. Solcova, Applied Catalysis B: Environmental 96 (2010) 239–244.
[17] N. Spataru, K. Tokuhiro, C. Terashima, T.N. Rao, A. Fujishima, Journal of Applied Electrochemistry 33 (2003) 1205–1210.
[18] T. Inoue, A. Fujishima, S. Konishi, K. Honda, Nature 277 (1979) 637–638.
[19] E.E. Barton, D.M. Rampulla, A.B. Bocarsly, Journal of the American Chemical Society 130 (2008) 6342–6344.
[20] S. Kaneco, Y. Ueno, H. Katsumata, K.T. Suzuki, K. Ohta, Chemical Engineering Journal 148 (2009) 57–62.
[21] M. Halmann, Nature 275 (1978) 115–116.
[22] T. Arai, S. Sato, K. Uemura, T. Morikawa, T. Kajino, T. Motohiro, Chemical Communications 46 (2010) 6944–6946.
[23] S. Kaneco, Y. Shimizu, K. Ohta, T. Mizuno, Journal of Photochemistry and Photobiology A: Chemistry 115 (1998) 223–226.
[24] K. Ito, S. Ikeda, M. Yoshida, S. Ohta, T. Iida, Bulletin of the Chemical Society of Japan 57 (1984) 583–584.
[25] H. Yoneyama, K. Sugimura, S. Kuwabata, Journal of Electroanalytical Chemistry and Interfacial Electrochemistry 249 (1988) 143–153.
[26] H. Flaisher, R. Tenne, M. Halmann, Journal of Electroanalytical Chemistry 402 (1996) 97–105.
[27] M.G. Bradley, T. Tysak, D.J. Graves, N.A. Viachiopoulos, Chemical Communications (1983) 349–350.
[28] B. Aurian-Blajeni, M. Halmann, J. Manassen, Solar Energy Materials 8 (1983) 425–440.
[29] H. Lin, A.K. Rumaiz, M. Schulz, C.P. Huang, S.I. Shah, Journal of Applied Physics 107 (2010) 124305–124306.
[30] G.R. Dey, Journal of Natural Gas Chemistry 16 (2007) 217–226.
[31] K. Koci, L. Obalova, O. Solcova, Chemical and Process Engineering 31 (2010) 395–407.
[32] Y.L. Lin, P.Y. Wang, L.L. Hsieh, K.H. Ku, Y.T. Yeh, C.H. Wu, Journal of Chromatography A 1216 (2009) 6377–6381.
[33] J.P. Qu, X.G. Zhang, Y.G. Wang, C.X. Xie, Electrochemica Acta 50 (2005) 3576–3580.
[34] W.F. Jardim, C. Pasquini, J.R. Guimaraes, L.C. de Faria, Water Research 24 (1990) 351–354.
[35] H. Zhao, D. Jiang, S. Zhang, W. Wen, Journal of Catalysis 250 (2007) 102–109.
[36] K. Ohta, M. Kawamoto, T. Mizuno, D.A. Lowy, Journal of Applied Electrochemistry 28 (1998) 717–724.
[37] X. Zhao, Y.F. Zhu, Environmental Science and Technology 40 (2006) 3367–3372.
[38] G. Hochgesand, Industrial and Engineering Chemistry 62 (1970) 37–43.
[39] J. Xia, M. Jodecke, A.P.-S. Kamps, G. Maurer, Journal of Chemical and Engineering Data 49 (2004) 1756–1759.
[40] G. Rothenberger, J. Moser, M. Graetzel, N. Serpone, D.K. Sharma, Journal of the American Chemical Society 107 (1985) 8054–8059.
[41] V.K. Mahajan, S.K. Mohapatra, M. Misra, International Journal of Hydrogen Energy 33 (2008) 5369–5374.
[42] A. Wolcott, W.A. Smith, T.R. Kuykendall, Y.P. Zhao, J.Z. Zhang, Advanced Functional Materials 19 (2009) 1849–1856.
[43] B. Zhou, M. Schulz, H.Y. Lin, S.I. Shah, J.H. Qu, C.P. Huang, Applied Catalysis B: Environmental 92 (2009) 41–49.
[44] S. Licht, Journal of Physical Chemistry B 105 (2001) 6281–6294.
[45] V. Chakrapani, J. Thangala, M.K. Sunkara, International Journal of Hydrogen Energy 34 (2009) 9050–9059.
[46] M. Subrahmanyam, S. Kaneco, N. Alonso-Vante, Applied Catalysis B: Environmental 23 (1999) 169–174.
[47] A. Naitoh, K. Ohta, T. Mizuno, H. Yoshida, M. Sakai, H. Noda, Electrochimica Acta 38 (1993) 2177–2179.
[48] S. Kaneco, N.-h. Hiei, Y. Xing, H. Katsumata, H. Ohnishi, T. Suzuki, K. Ohta, Journal of Solid State Electrochemistry 7 (2003) 152–156.
[49] S. Kaneco, K. Iiba, M. Yabuuchi, N. Nishio, H. Ohnishi, H. Katsumata, T. Suzuki, K. Ohta, Industrial and Engineering Chemistry Research 41 (2002) 5165–5170.
[50] S. Kaneco, H. Katsumata, T. Suzuki, K. Ohta, Energy Fuels 20 (2005) 409–414.
[51] S. Kaneco, Y. Ueno, H. Katsumata, T. Suzuki, K. Ohta, Chemical Engineering Journal 119 (2006) 107–112.
[52] T. Yui, A. Kan, C. Saitoh, K. Koike, T. Ibusuki, O. Ishitani, ACS Applied Materials and Interfaces 3 (2011) 2594–2600.
[53] N.M. Dimitrijevic, B.K. Vijayan, O.G. Poluektov, T. Rajh, K.A. Gray, H. He, P. Zapol, Journal of the American Chemical Society 133 (2011) 3964–3971.
[54] M. Anpo, Research on Chemical IntermediatesþV 11 (1989) 67–106.
[55] C.J. Willmott, S.G. Ackleson, R.E. Davis, J.J. Feddema, K.M. Klink, D.R. Legates, J. O'Donnell, C.M. Rowe, Journal of Geophysical Research 90 (1985) 8995–9005.
[56] Y.P. Peng, K.S. Chen, J.C. Lou, S.W. Hwang, W.C. Wang, C.H. Lai, M.Y. Tsai, Terrestrial Atmospheric and Oceanic Sciences 19 (2008) 505–514.
[57] Y. Zhang, J. Wan, Y. Ke, Journal of Hazardous Materials 177 (2010) 750–754.
[58] Y.P. Peng, S.L. Lo, F.H. Ou, S.W. Lai, Journal of Hazardous Materials 183 (2010) 754–758.